EDGE ARTICLE

Check for updates

Unraveling non-radiative decay channels of exciplexes to construct efficient red emitters for organic light-emitting diodes†

Heng-Yuan Zhang,[a] Ming Zhang,[a] Hao Zhuo,[a] Hao-Yu Yang,[a] Bo Han, [ID] *[b]
Yong-Hao Zheng, [ID] [a] Hui Wang,[c] Hui Lin, [ID] [a] Si-Lu Tao, [ID] [a] Cai-Jun Zheng [ID] *[a]
and Xiao-Hong Zhang [ID] *[c]

Exciplex emitters naturally have thermally activated delayed fluorescence characteristics due to their spatially separated molecular orbitals. However, the intermolecular charge transfer potentially induces diverse non-radiative decay channels, severely hindering the construction of efficient red exciplexes. Thus, a thorough comprehension of this energy loss is of paramount importance. Herein, different factors, including molecular rigidity, donor–acceptor interactions and donor–donor/acceptor–acceptor interactions, that impact the non-radiative decay were systematically investigated using contrasting exciplex emitters. The exciplex with rigid components and intermolecular hydrogen bonds showed a photoluminescence quantum yield of 84.1% and a singlet non-radiative decay rate of 1.98×10^6 s^{-1} at an optimized mixing ratio, respectively, achieving a 3.3-fold increase and a 70% decrease compared to the comparison group. In the electroluminescent device, a maximum external quantum efficiency of 23.8% was achieved with an emission peak of 608 nm, which represents the state-of-the-art organic light-emitting diodes using exciplex emitters. Accordingly, a new strategy is finally proposed, exploiting system rigidification to construct efficient red exciplex emitters that suppress non-radiative decay.

Introduction

Excited complexes, known as exciplexes, have been considered detrimental to the efficiency of organic light-emitting diodes (OLEDs) since Karasz *et al.* first observed the unexpected and extra red-shifted emission in 1994.[1] It was not until 2012 when Adachi and coworkers[2] reported the thermally activated delayed fluorescence (TADF) characteristics of some exciplexes that researchers began to probe their applications in OLEDs.[3–9] Formed by mixing electron donors and electron acceptors (D : A) to generate intermolecular charge-transfer (CT) states, the exciplexes possess small singlet–triplet energy gaps (ΔE_{ST}s) because of the spatially separated highest occupied molecular orbital (HOMO) and lowest unoccupied molecular orbital (LUMO), which promotes the reverse intersystem crossing

(RISC), converting dark triplet excitons to singlet excitons. Benefiting from the theoretical 100% exciton utilization, TADF exciplex emitters are promising to achieve efficient electroluminescence (EL).

Over the past decade, with considerable efforts in molecular design and combination optimization of D : A pairs, blue and green OLEDs that utilize exciplex emission have realized remarkable maximum external quantum efficiencies (EQE$_{max}$s) of 20.43%[10] and 26.4%,[11] respectively. However, the efficiency of red exciplex emitters is far from satisfactory. The highest EL efficiency to date was contributed by Cheng *et al.*, realizing an EQE$_{max}$ of 14.6% with an emission peak at 592 nm.[12] When the emission peak is limited to wavelengths redder than 600 nm, the highest EQE$_{max}$ (8.68%) was achieved by using a manganese-based donor and a beryllium-based acceptor.[13] Besides, researchers combined stronger donors and acceptors for deep-red and near-infrared emission, but the EQE$_{max}$s were less than 5%.[14–16] As summarized above, a clear trend can be observed, that is, a sharp decrease in efficiency with the redshift of emission, which can be mainly ascribed to the exponentially increasing non-radiative energy loss as the energy gap gets smaller.[17] Therefore, the inhibition of such energy loss is imperative in realizing efficient red exciplexes, as evidenced by the extensive research on single-molecule red TADF emitters.[18–20] Theoretically, the emission process of an exciplex can be described as:[5]

[a]School of Optoelectronic Science and Engineering, University of Electronic Science and Technology of China, Chengdu 611731, P. R. China. E-mail: zhengcaijun@uestc.edu.cn

[b]Chengdu University of Traditional Chinese Medicine, State Key Laboratory Southwestern Chinese Medicine Resources, Chengdu 611137, P. R. China. E-mail: hanbo@cdutcm.edu.cn

[c]Institute of Functional Nano & Soft Materials (FUNSOM), Soochow University, Suzhou 215123, P. R. China. E-mail: xiaohong_zhang@suda.edu.cn

$$D + A + h\nu \rightarrow A^* + D \text{ or } A + D^* \rightarrow (A^{\delta-}D^{\delta+})^* \rightarrow$$
$$h\nu_{\text{exciplex}} + A + D \quad (1)$$
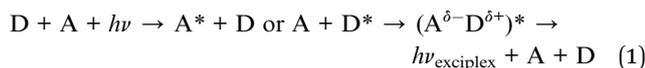
where a donor (or an acceptor) is excited first and then collides with a ground-state acceptor (or donor) to generate CT states prior to the final emission. All the processes should be taken into account to study the emission mechanisms of exciplexes.[7,21] As a result, the non-radiative decay should be considered during the excitation of D or A, the CT between D and A molecules and the final radiation. The properties of the constituting molecules and the D–A intermolecular interactions are therefore influential in the exciplex emission.[8] Besides, as the mixing ratios of D and A in an exciplex system are generally similar (many are even mixed in equal proportions), the non-radiative energy loss caused by concentration quenching should also be noticed, especially for red exciplexes where the efficiency is substantially constrained by such energy loss. Consequently, the D : A-type exciplex emitters potentially possess more non-radiative decay channels (Fig. 1A) compared with the single-molecule TADF emitters. And it is of vital significance to unravel specific paths and propose effective strategies to construct efficient red exciplex emitters.

In this work, we systematically investigate non-radiative decay channels of red exciplex emitters using contrasting D : A pairs and propose an effective strategy accordingly. As shown in Fig. 1B, two donors and three acceptors were developed using phenoxazine/phenothiazine (PXZ/PTZ) and N-heterocycles to achieve red emission, and all six exciplexes show emission peaks around 600 nm. The three acceptors are distinguished by

their attachments that the spiro-locked **SAF-2NP** is much more rigid than triphenylamine (TPA)-based **TPA-2NP** and **TPA-QP**. Additionally, the regulation of intermolecular interactions between D and A molecules was achieved by strategic molecular design. Intermolecular hydrogen bonds (HBs) between PXZ and 2NP were found in **mPTBC : SAF-2NP** and **mPTBC : TPA-2NP** because of the exposed electronegative sites, while **mPTBC : TPA-QP**, **mPTZC : SAF-2NP**, **mPTZC : TPA-2NP** and **mPTZC : TPA-QP** lack the corresponding interactions. It was found that both suppressing the structural relaxation of exciplex components and strengthening the D–A interactions are beneficial for restricting non-radiative decay. Owing to the synergy of stable structures and intermolecular HBs, **mPTBC : SAF-2NP** showed the lowest k_{nr} (singlet non-radiative decay rate, $1.98 \times 10^6 \text{ s}^{-1}$) and the largest photoluminescence quantum yield (PLQY, 84.1%) among the six exciplexes. Furthermore, the D–D/A–A interactions were studied. Suffering from exciton quenching caused by π–π stacking of **SAF-2NP**, the k_{nr} of **mPTBC : SAF-2NP** gradually increased as the acceptor concentration increased. The concentration quenching was much more severe in TPA-containing exciplex emitters. Moderate efficiency declines of **mPTBC : SAF-2NP**-based devices were observed where EQE$_{max}$s maintain above 20% with the D : A ratio from 9 : 1 to 6 : 4. At the optimized ratio, an outstanding EQE$_{max}$ of 23.8% with an emission peak at 608 nm was obtained, which not only surpasses all previously reported red exciplex OLEDs but also ranks among state-of-the-art exciplex-emissive devices. Based on the above results, we elucidate that the molecular rigidity, D–D/A–A interactions and D–A interactions are three factors that impact the non-radiative decay. Accordingly, we propose a new strategy leveraging a rigid system featuring stiff structures, intermolecular HBs and optimized D : A ratios to construct red exciplex emitters that effectively suppress the non-radiative decay. The present work provides perspectives to understand the non-radiative decay paths and is helpful in elucidating the emission mechanisms of exciplex emitters.

Results and discussion

Exciplex construction and molecular characterization

The donor–acceptor structure was applied to construct exciplex constituents, which induces TADF characteristics and thus improves exciton utilization of exciplex systems. **mPTBC** was constructed by incorporating PXZ onto a sterically crowded group. The V-shaped tri-benzonitrile, on the one hand, obstructs the rotation of PXZ and minimizes the structure deformation, and on the other hand prevents planar PXZ from π–π stacking. The acceptor **SAF-2NP** was a bulky and planar N-heterocycle modified with an sp³ hybridized carbon mediated orthogonal spiro-acridine unit, which locks the rotational peripheries. To regulate the constituent rigidity and D–A intermolecular interactions, as for the donor, PTZ is substituted for PXZ to produce **mPTZC**, resulting in a decrease in electronegativity[22] and a moderate alteration in the HOMO energy level. This greatly lowers the possibility of HB formation since weak HBs are dominated by electrostatic interactions.[23] As for the acceptors, by replacing SAF with the TPA unit, the structural
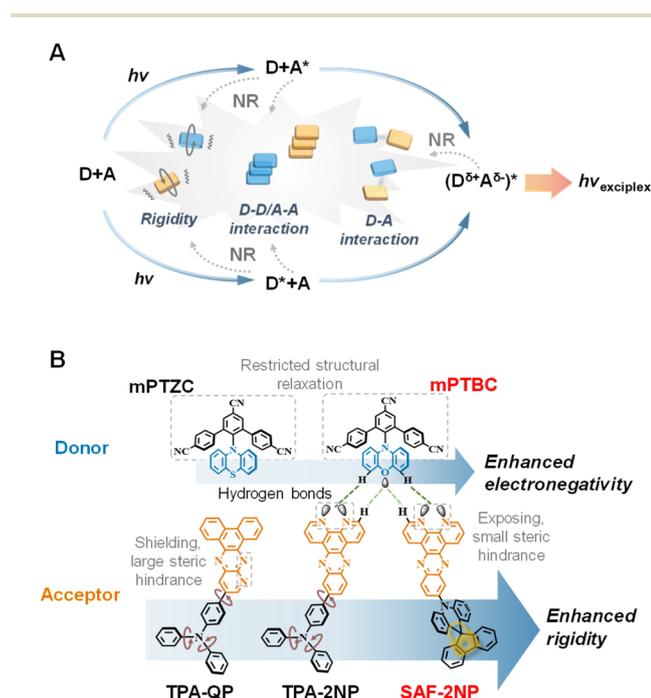

Fig. 1 (A) Illustration of the emission process of exciplex emitters and three factors that can lead to non-radiative decay of exciplex emitters. D stands for donors, A represents acceptors and NR is non-radiative decay. (B) Design concept and the corresponding molecular structures of donors and acceptors.

stability is greatly impaired because of the rotatable attachments and reduced steric hindrance between TPA and 2NP/QP.[24] In addition, the position of nitrogen atoms of QP is elaborately modified from exposing to shielding sites of the molecule (Fig. 1B), generating large steric hindrance for HB formation compared with 2NP.

2′-(10H-Phenoxazin-10-yl)-[1,1′:3′,1″-terphenyl]-4,4″,5′-tricarbonitrile (**mPTBC**),[25] 10-(dipyrido[3,2-a:2′,3′-c]phenazin-11-yl)-10H-spiro[acridine-9,9′-fluorene] (**SAF-2NP**),[26] 4-(dipyrido[3,2-a:2′,3′-c]phenazin-11-yl)-N,N-diphenylaniline (**TPA-2NP**)[27] and 4-(dibenzo[f,h]pyrido[2,3-b]quinoxalin-12-yl)-N,N-diphenylaniline (**TPA-QP**)[28] were synthesized according to previous reports. 2′-(10H-Phenoxazin-10-yl)-[1,1′:3′,1″-terphenyl]-4,4″,5′-tricarbonitrile (**mPTZC**) was readily synthesized using the same procedure as **mPTBC**, including the Suzuki coupling, diazotization reaction and C–N cross-coupling of tri-benzonitrile and PTZ. Column chromatography, recrystallization and sublimation were used to obtain appreciable purity. Its chemical structure was fully characterized through ^{1}H and ^{13}C nuclear magnetic resonance (NMR) spectroscopy and mass spectrometry. The basic physical properties of donors and acceptors were characterized first (summarized in Table S1†). Thermogravimetric analysis (TGA) and differential scanning calorimetry (DSC; Fig. S1†) tests were conducted to evaluate the thermal stability of **mPTZC**. The decomposition temperature (corresponding to 5% weight loss) of **mPTZC** was calculated to be 381 °C, and no glass transition was observed. As shown in Fig. S2,† **mPTZC**, **TPA-2NP** and **TPA-QP** show clear CT absorption and emission peaks around 430 nm and 540 nm, respectively. According to the fluorescence and phosphorescence spectra, **TPA-2NP** and **TPA-QP** possess relatively large ΔE_{ST}s due to the large conjugation, similar to other TPA-based TADF emitters.[19,29,30] In contrast, twisted structures of **mPTBC**, **mPTZC** and **SAF-2NP** induce tiny ΔE_{ST}s, which may further affect the fluorescence lifetime and RISC rates of the corresponding exciplexes. Estimated according to the reduction and oxidation curves (Fig. S3†) obtained by the cyclic voltammetry method, **SAF-2NP**, **TPA-2NP** and **TPA-QP** have similar LUMO energy levels of −3.32 eV, −3.27 eV and −3.31 eV, respectively. **mPTBC** and **mPTZC** show similar HOMO energy levels, making the corresponding exciplex emitters comparable. The fluorescence spectra of the six exciplex emitters and their electron-donating and electron-accepting components are displayed in Fig. S4 and S5.† Emission peaks at around 600 nm were observed for all six exciplexes, exhibiting clear red shifts compared with those of their constituents, confirming the exciplex formation.[31] The emission energy is in accordance with the differences between HOMO energy levels of donors and LUMO energy levels of acceptors (listed in Table S1†).

Molecular rigidity and intermolecular interactions

In order to theoretically distinguish the rigidity of these compounds, density functional theory (DFT) and time dependent DFT (TD-DFT) were conducted using Gaussian.[32] As shown in Fig. 2A, optimized geometries of the ground state (S_0), the lowest singlet excited state (S_1) and the lowest triplet state (T_1) as well as the corresponding root-mean-square displacements (RMSDs) of all five components were calculated using VMD[33] in
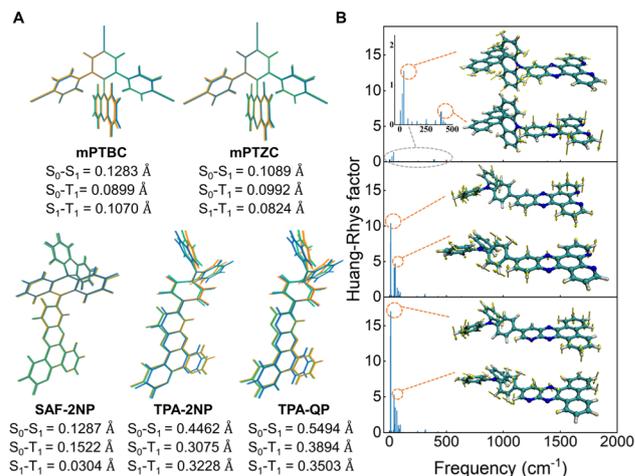

Fig. 2 (A) S_0, S_1 and T_1 (in blue, orange and green, respectively) geometry variations of the five monomers and the corresponding RMSD values. (B) Calculated S_0–S_1 Huang–Rhys factors of **SAF-2NP** (upper), **TPA-2NP** (middle) and **TPA-QP** (lower) at different frequencies (inset: representative vibrational modes).

the first place. There is little geometry change between the ground state and excited states for **mPTBC** and **mPTZC**, indicating that the V-shaped tri-benzonitrile effectively stabilizes the molecules. As for the acceptors, RMSD show a prominently decreasing trend from **TPA-QP** to **SAF-2NP**, indicating suppressed structural relaxation. These larger values of TPA-modified acceptors mainly arise from the dihedral angle change between TPA and 2NP/QP as well as the rotation of peripheral phenyl. To further study the structural deformation, Huang–Rhys factors at different normal mode frequencies of the three acceptors were calculated according to the reorganization energy using the DUSHIN program,[34] and the results are demonstrated in Fig. 2B and S6.† The Huang–Rhys factor of **SAF-2NP** is significantly smaller than those of **TPA-2NP** and **TPA-QP**. As shown by the inset in Fig. 2B, the most and second most representative normal modes of **SAF-2NP** correspond to wagging vibrations of the acridine unit (38 cm^{-1}) and C–H as well as C–C twisting vibrations of the 2NP plane (396 cm^{-1}). However **TPA-2NP** and **TPA-QP** possess similar twisting vibration modes resulting in rotations between the peripheral phenyl and the acceptor plane (12 cm^{-1}) as well as rotations between the acceptor plane and adjacent phenyl (51 cm^{-1}). Besides, the primary vibrations that contribute to the reorganization energy of **SAF-2NP** and TPA-derivatives, respectively, belong to the high-frequency region which corresponds to the bond length change and the low-frequency region that relates to the dihedral angle change (Fig. S6†).[24] The relatively smaller reorganization energy of **SAF-2NP** is derived from the effective suppression of low-frequency vibrations. The above data well support our molecular design that **SAF-2NP** is rigidified by restricting D–A rotations using acridine with large steric hindrance and locking the flexible benzene with fluorene. Therefore, it is rational to explore the influence of structural stiffness on the non-radiative decay of exciplexes using **SAF-2NP**, **TPA-2NP** and **TPA-QP** as acceptors.

Moreover, the D–A intermolecular interactions were investigated experimentally and theoretically. Based on our molecular design concept, **mPTZC** and **TPA-QP** cannot form the desired intermolecular HBs in exciplex systems. The assumption was initially verified using fitted atomic charges of the five molecules. As shown in Fig. S7,† although the maximum hydrogen charges of **mPTBC** and **mPTZC** are similar, respectively, located near oxygen and sulfur, the oxygen charge is two times more negative than the sulfur charge, providing feasibility for stronger interactions. For **SAF-2NP** and **TPA-2NP**, nitrogen atoms in phenanthroline have the most negative charges, and the exposed sites benefit the formation of intermolecular HBs between PXZ and 2NP in **mPTBC : SAF-2NP** and **mPTBC : TPA-2NP**. In contrast, the electronegative nitrogen atoms of **TPA-QP** are shielded by TPA and phenanthrene groups, generating large steric hindrance. The restrained electrostatic potential (RESP) was also used (Fig. S8†), which showed good consistency with the MK method. Fourier Transform Infrared (FT-IR) spectra were recorded to make experimental validation (Fig. S9†). New absorption peaks at 2967 and 2962 cm^{-1} are, respectively, observed for **mPTBC : SAF-2NP** and **mPTBC : TPA-2NP**, which are shifted from the C–H stretching modes (around 3059 cm^{-1}), demonstrating the existence of intermolecular HBs.[35,36] Meanwhile, the spectra of the other four blends are the superposition of the components. To better illustrate the intermolecular interactions of **mPTBC : SAF-2NP** and **mPTBC : TPA-2NP**, the independent gradient model based on Hirshfeld partition (IGMH)[37] analysis was carried out using Multiwfn[38] based on the optimized geometries. As shown in Fig. 3A, B, D and E, the blue region in the isosurface and scatter plots denotes attractive interaction and the green region represents dispersion-dominant interaction. Prominent C–H⋯N intermolecular HBs are observed with the participation of the active hydrogen next to oxygen and two strong-electronegative nitrogen atoms (Fig. S10†). The central area of the C–H⋯O isosurface appears light blue, indicating that the interactions are weaker than C–H⋯N, but it is also helpful to stabilize the exciplex system. The interaction energy was, respectively, calculated to be −10.09 and −10.19 kcal mol^{-1} for **mPTBC : SAF-2NP** and **mPTBC : TPA-2NP** considering the basis set superposition error (BBSE), which is in a range of weak intermolecular HBs.[23] The interaction region in the electrostatic potential (ESP) map[39] (Fig. 3C and F) exhibits red-blue crossings, in line with the previous report that weak HBs are dominated by electrostatic interaction. Intermolecular HBs may benefit the interactions between D and A molecules, facilitating the exciplex formation. Moreover, the exciplex systems can be stabilized, weakening the non-radiative decay.

Based on the above analysis, molecular rigidity and intermolecular interactions are modified by elaborate molecular design. And the pairwise combination of D : A can be fitted into the following four scenarios. **mPTBC : TPA-QP**, **mPTZC : TPA-2NP** and **mPTZC : TPA-QP** contain relatively flexible TPA segments. Besides, the weak electronegativity of sulfur in **mPTZC** and shielding nitrogen in **TPA-QP** impede the formation of desired HBs. Therefore, these three exciplexes stand for circumstances that lack both constituent rigidity and effective intermolecular HBs. Likewise, **mPTZC : SAF-2NP** is expected to have no intermolecular HBs between PTZ and 2NP, while good rigidity is anticipated. **mPTBC : TPA-2NP** possesses favorable HBs but serious structural relaxation. Impressively, both were achieved for the proof-of-concept **mPTBC : SAF-2NP**, which is expected to effectively inhibit the non-radiative decay and achieve efficient red emission.

Photophysical properties

The transient photophysical properties of the six exciplexes were then characterized to study the exciton dynamics. Given the twisted structure of donors and planar geometry of
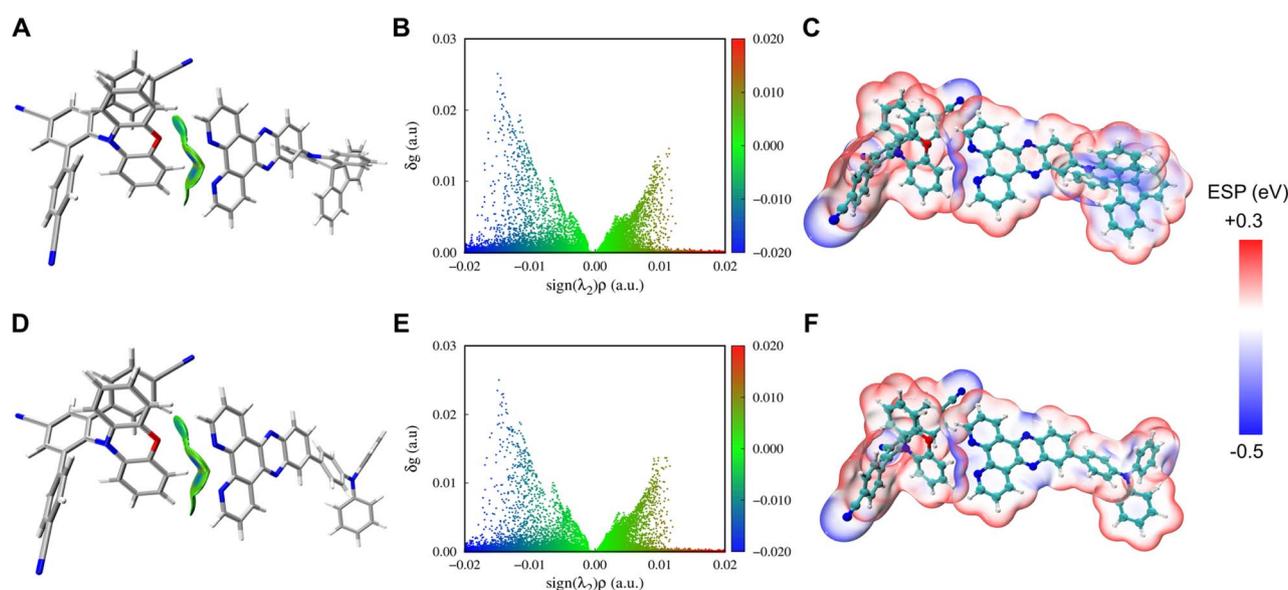

Fig. 3 Isosurface maps of intermolecular interaction based on optimized geometry (isovalue = 0.003 a.u., color range: ± 0.02 a.u.), corresponding scatter plots and ESP maps of **mPTBC : SAF-2NP** (A–C) and **mPTBC : TPA-2NP** (D–F).
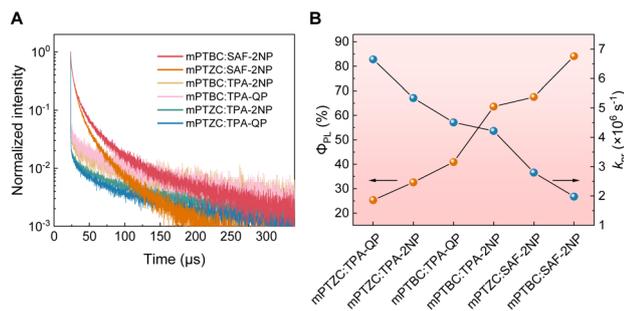
Fig. 4 (A) PL decay curves of mPTBC : SAF-2NP, mPTZC : SAF-2NP, mPTBC : TPA-2NP, mPTBC : TPA-QP, mPTZC : TPA-2NP and mPTZC : TPA-QP. (B) Variation trends of Φ_{PL} and k_{nr} from mPTZC : TPA-QP to mPTBC : SAF-2NP (D : A = 9 : 1).

acceptors, the D : A mixing ratio for all six exciplexes was set to be 9 : 1 in the first place to avoid concentration quenching. As shown in Fig. 4A and S9† and Table 1, the nanosecond-scale prompt decay lifetime (τ_p) and microsecond-scale delayed fluorescence lifetime (τ_d) were obtained for all six exciplexes, validating their TADF characteristics. Note that the multiple RISC channels in all six exciplex systems lead to complexity of the emission processes.[40] Herein, we focus on the overall decay characteristics rather than the classification of specific emitting species. TPA-containing exciplexes have larger τ_ds, which can be ascribed to their larger ΔE_{ST}s (Fig. S12†). And the longer τ_ds of **TPA-2NP** and **TPA-QP** compared with that of **SAF-2NP** (Fig. S13†) are also responsible for the longer τ_ds of TPA-containing exciplexes since this leads to longer triplet lifetimes in the exciplex systems. The significantly smaller τ_d of **SAF-2NP** compared with those of TPA-based acceptors contributes to shorter τ_ds of **mPTBC : SAF-2NP** (22.3 µs) and **mPTZC : SAF-2NP** (17.5 µs). An increasing trend of Φ_{PL} and a decreasing trend of k_{nr} were observed from **mPTZC : TPA-QP** to **mPTBC : SAF-2NP**, as shown in Fig. 4B. **mPTBC : TPA-QP**, **mPTZC : TPA-2NP** and **mPTZC : TPA-QP** have large k_{nr}s, and non-radiative decay is gradually reduced after introducing HBs (**mPTBC : TPA-2NP**) and the stiff acceptor (**mPTZC : SAF-2NP**). **mPTBC : SAF-2NP** possesses the smallest k_{nr}. Specifically, in terms of structure rigidification, k_{nr}s are, respectively, decreased by 57.9% and 47.6% from **mPTZC : TPA-QP** (6.65×10^6 s^{-1}) and **mPTZC : TPA-2NP** (5.34×10^6 s^{-1}) to **mPTZC : SAF-2NP** (2.80×10^6 s^{-1}). Similarly, a drop rate of 53.1% is obtained from **mPTBC : TPA-2NP** to **mPTBC :**

SAF-2NP. These improvements can be attributed to the bulky acridine and periphery-locking fluorene, which effectively curbs the structural deformation. **TPA-QP**-based exciplexes have larger k_{nr}s than those containing **TPA-2NP**, which can be ascribed to more severe structural relaxation of **TPA-QP** (Fig. 2). Comparatively, the introduction of HBs has less effect on k_{nr}. It is, respectively, decreased by 29.3% and 6.4% from **mPTZC : SAF-2NP** (2.80×10^6 s^{-1}) to **mPTBC : SAF-2NP** (1.98×10^6 s^{-1}) and from **mPTBC : TPA-QP** (4.51×10^6 s^{-1}) to **mPTBC : TPA-2NP** (4.22×10^6 s^{-1}). This experimentally validates our assumption that intermolecular HBs can rigidify the exciplex systems and weaken non-radiative decay. The enhancement of k_f of **mPTBC : TPA-2NP** compared with that of **mPTZC : SAF-2NP** may originate from the large conjugation of **TPA-2NP**. Remarkably, **mPTBC : SAF-2NP** has the largest Φ_{PL} of 84.1% and the smallest k_{nr}, showing a 3.3-fold increase and a 70% decrease compared with those of **mPTZC : TPA-QP**. According to these results, improving the component stiffness has a dramatic impact on the non-radiative decay of the exciplex systems, while intermolecular HBs have relatively moderate influence and barely work for systems that lack sufficient structural stability. The impressive performance of **mPTBC : SAF-2NP** highlights the significance of the synergy of rigid structures and strong intermolecular interactions that effectively suppress the non-radiative transition.

According to the above studies, the molecular rigidity of red exciplex emitters is the basis for suppressing non-radiative decay. Planar structures are therefore hard to avoid and the consequent concentration quenching would be no longer negligible. Steady-state PL spectra, Φ_{PL} and transient PL curves of **mPTBC : SAF-2NP** with D : A ratios from 9 : 1 to 6 : 4 were measured. Both τ_p and τ_d remain nearly identical (Fig. S14 and Table S2†) with increasing concentration of **SAF-2NP**. However Φ_{PL} shows a decreasing trend, making k_{nr} gradually increase from 1.98×10^6 s^{-1} to 2.72×10^6 s^{-1}. The photophysical properties of other five exciplexes with different D : A ratios were also studied (Fig. S15 and Table S3†). The k_{nr}s of TPA-containing exciplexes are much more sensitive to the concentration, demonstrating 1.2–1.7-fold increases from D : A = 9 : 1 to 8 : 2. However the concentration of **SAF-2NP** has smaller alterations.

To understand these results, the crystal structures and corresponding packing modes of **mPTBC** (CCDC 2343106), **SAF-2NP** (CCDC 2343111) and **TPA-QP** (CCDC 2370557) are

Table 1 Summary of photophysical properties of the six exciplexes

Emitter	$\lambda_{PL}^{a,b}$ [nm]	$\Phi_{PL}^{b,c}$ [%]	τ_p^{b} [ns]	τ_d^{b} [µs]	k_f [10^6 s^{-1}]	k_{ISC}^{d} [10^7 s^{-1}]	k_{RISC}^{e} [10^5 s^{-1}]	k_{nr}^{f} [10^6 s^{-1}]
mPTBC : SAF-2NP	610	84.1	20.7	22.3	10.50	3.57	1.74	1.98
mPTZC : SAF-2NP	608	67.5	23.2	17.5	5.82	3.43	2.86	2.80
mPTBC : TPA-2NP	596	63.6	18.7	65.2	7.04	4.18	0.71	4.22
mPTBC : TPA-QP	610	40.9	21.3	59.6	3.12	3.92	1.03	4.51
mPTZC : TPA-2NP	600	32.6	15.5	77.7	2.58	5.65	1.05	5.34
mPTZC : TPA-QP	608	25.3	13.9	62.6	2.25	6.29	1.29	6.65

[a] Emission peaks of fluorescence spectra. [b] Measured with exciplex solid films (D : A = 9 : 1). [c] Measured in a nitrogen atmosphere. [d] Intersystem crossing rate constant. [e] RISC rate constant. [f] Singlet non-radiative decay rate constant.

demonstrated. As shown in Fig. S16,† for **mPTBC**, the stacking of PXZ is effectively avoided by the two carbonitrile arms. No π–π interactions but only C–H···N and C–H···π interactions were observed. For the acceptors (Fig. S17†), **SAF-2NP** has head-to-tail stacking with larger intermolecular distances of ∼3.33 and ∼3.45 Å, while **TPA-QP** shows head-to-head off-center parallel stacking with intermolecular distances of ∼3.27 Å. As the acceptor concentration increases, more serious π–π stacking and thus more severe energy loss can be anticipated. Therefore, all six exciplexes showed greater k_{nr} when the acceptor concentration increases. In particular, **SAF-2NP**-based exciplex emitters are less sensitive owing to the nearly perpendicular structure of SAF.

OLED devices

Considering the dramatic contrast in the PL properties of the six exciplexes, their EL properties were then investigated. As shown in Fig. 5A, a simple multi-layer device structure of ITO (110 nm)/ TPAC (35 nm)/TCTA (10 nm)/emitting layer (EML, 20 nm)/ TmPyPB (65 nm)/LiF (1 nm)/Al (100 nm) was used, where 4,4′-(cyclohexane-1,1-diyl)bis(N,N-di-p-tolylaniline) (TAPC), tris(4-(9H-carbazol-9-yl)phenyl)amine (TCTA) and 3,3′-(5′-(3-(pyridin-3-yl)phenyl)-[1,1′:3′,1″-terphenyl]-3,3″-diyl)dipyridine (TmPyPB) were hole transporting, electron blocking and electron transporting layers, respectively (for chemical structures, see Fig. S18†). Indium tin oxide (ITO) and Al, respectively, served as the anode and cathode. LiF improved electron injection. Devices A–F represent the EML using **mPTBC : SAF-2NP**, **mPTZC : SAF-2NP**, **mPTBC : TPA-2NP**, **mPTBC : TPA-QP**, **mPTZC : TPA-2NP** and

mPTZC : TPA-QP, respectively. As mentioned above, the D : A weight ratio was set to be 9 : 1 in the first place to suppress the π–π stacking of the acceptors. **mPTBC : SAF-2NP**-based OLEDs demonstrate the highest maximum luminance (Fig. 5B), which can be ascribed to their superior structural stability. The higher electron transport ability of **TPA-2NP** endows **TPA-2NP**-based devices with higher current density than those based on **TPA-QP** (Fig. S19†). According to the EL spectra in Fig. 5C, all six exciplex-based OLEDs exhibited red emission that peaked around 600 nm, similar to their PL spectra. Due to the serious non-radiative decay mainly induced by the flexible TPA group, devices D, E and F showed poor EQE_{max}s of 9.34%, 8.55% and 5.58%, respectively. Excitingly, devices B and C demonstrated obvious performance enhancement and achieved a maximum CE/PE/EQE of 24.3 cd A^{-1}/25.8 lm W^{-1}/12.5% and 19.6 cd A^{-1}/ 16.4 lm W^{-1}/14.1%, respectively (Fig. 5D and Table 2). Consistent with what have been concluded from the PL properties, it is further verified that structural robustness is the priority in constructing high-performance red exciplex emitters, which is demonstrated by more significant improvements after rigidifying the molecules (from **mPTZC : TPA-2NP** to **mPTZC : SAF-2NP**), as compared with introducing HBs (from **mPTBC : TPA-QP** to **mPTBC : TPA-2NP**). The proof-of-concept **mPTBC : SAF-2NP** achieved exceptionally maximum CE, PE and EQE of 41.5 cd A^{-1}, 34.7 lm W^{-1} and 23.8%, respectively, showing a 4.2-fold improvement in EQE_{max} compared with that of **mPTZC : TPA-QP**. These results not only take a huge lead to previously reported red OLEDs based on exciplex emitters (Fig. 5E)[41–46] but also ranks among the state-of-the-art exciplex-emissive OLEDs (Fig. S20, Table S6†). Furthermore, OLEDs with different D : A
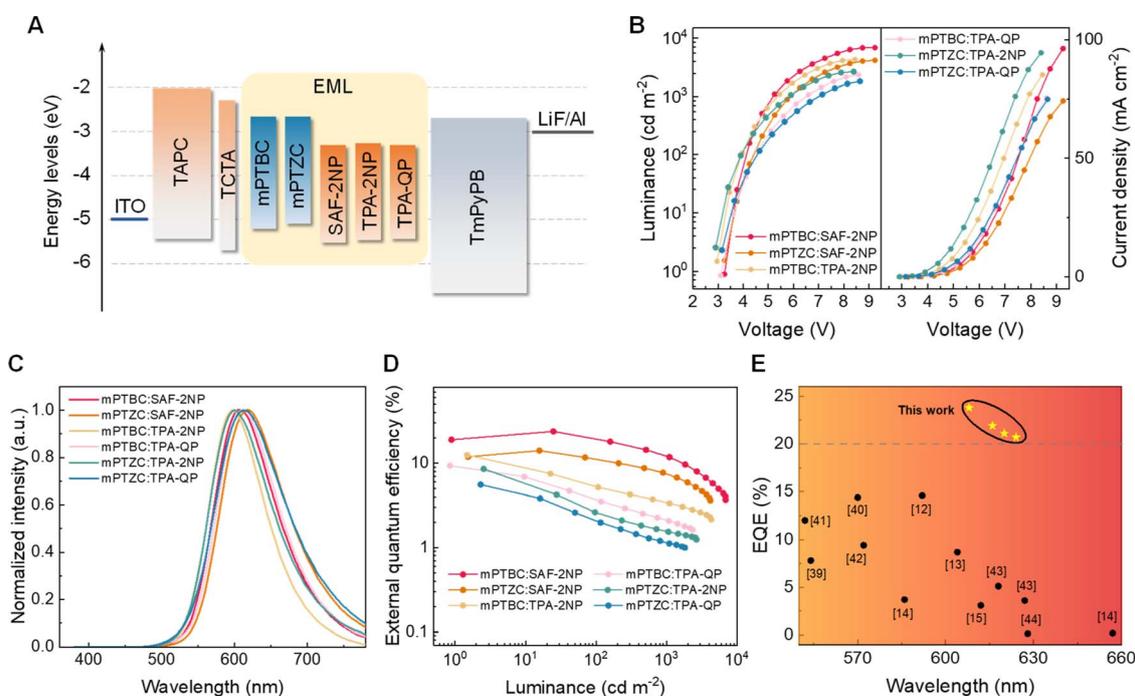

Fig. 5 (A) Device configuration of the exciplex-based OLEDs. Luminance–voltage–current density curves (B), EL spectra (C) and EQE–luminance plot (D) of **mPTBC : SAF-2NP**, **mPTBC : TPA-2NP**, **mPTBC : TPA-QP**, **mPTZC : SAF-2NP**, **mPTZC : TPA-2NP** and **mPTZC : TPA-QP**. (E) EQE vs. wavelength plot of representative yellow to deep-red OLEDs based on exciplex emitters.

Table 2 Summary of EL performance based on the six exciplexes

Device	Emitter	Weight ratio	V_{on}^{a} [V]	λ_{EL}^{b} [nm]	Maximum CE/PE/EQE [cd A^{-1}/lm W^{-1}/%]	EQE$_{100}$/EQE$_{500}$/EQE$_{1000}^{c}$ [%]	CIE^{b} [x, y]
A1	**mPTBC : SAF-2NP**	9 : 1	3.3	608	41.5/34.7/23.8	19.3/14.5/12.1	(0.58, 0.42)
A2		8 : 2	3.1	616	31.2/27.2/21.9	17.6/13.4/11.2	(0.61, 0.39)
A3		7 : 3	3.0	620	26.8/24.0/21.1	17.1/13.3/11.3	(0.62, 0.38)
A4		6 : 4	3.0	624	24.3/21.8/20.7	17.3/13.4/11.3	(0.63, 0.37)
B	**mPTZC : SAF-2NP**	9 : 1	3.2	620	19.6/16.4/14.1	11.1/8.7/7.4	(0.60, 0.40)
C	**mPTBC : TPA-2NP**	9 : 1	2.9	596	24.3/25.8/12.5	5.3/3.9/3.4	(0.56, 0.43)
D	**mPTBC : TPA-QP**	9 : 1	3.1	612	13.3/13.5/9.34	3.7/2.5/2.1	(0.58, 0.41)
E	**mPTZC : TPA-2NP**	9 : 1	2.8	600	14.5/15.7/8.55	2.6/1.8/1.6	(0.56, 0.44)
F	**mPTZC : TPA-QP**	9 : 1	3.1	612	7.51/7.48/5.58	2.1/1.3/1.1	(0.56, 0.43)

^{a} Driving voltage at 1 cd m^{-2}. ^{b} At 500 cd m^{-2}. ^{c} EQE at 100, 500 and 1000 cd m^{-2}.

mixing ratios were then fabricated to study the effect of D–D/A–A interactions on device performances. For **mPTBC : SAF-2NP**, devices A1–A4 were fabricated with D : A ratios of 9 : 1, 8 : 2, 7 : 3 and 6 : 4, respectively. The spectral redshifts are due to the synergistic effect of increased π–π interactions of **SAF-2NP** and the self-polarization-induced solid-state solvation effect caused by larger dipole moments of **SAF-2NP** (1.80 debye) than those of **mPTBC** (0.055 debye).[29] The EQE$_{max}$s gradually decreased with the increase in the acceptor concentration (Fig. S21,† Table 2), showing a similar trend to that observed in photophysical studies, which should be ascribed to exciton quenching due to the π–π interactions of **SAF-2NP**. Despite this, EQE$_{max}$s of the four devices remain above 20%, with emission peaks ranging from 608 to 624 nm, demonstrating superiority to those concentration-sensitive single-component TADF red emitters.[29,30,47–49] The device performances based on other five emitters with different D : A mixing ratios are shown in Fig. S22 and S23 and Table S5.† Similarly, **mPTZC : SAF-2NP** also shows moderate concentration quenching with EQE$_{max}$s decreasing from 14.1% to 11.9% as the acceptor concentration increases to 20%. Conversely, TPA-containing exciplex emitters demonstrate significant EQE$_{max}$ decline with drop rates ranging from 45.7% to 56.7%, indicating that TPA-based acceptors are much more sensitive to concentration and are prone to π–π stacking, which is consistent with their photophysical properties. Based on the above studies, the outstanding performance of device A1 is the result of effectively suppressing the non-radiative decay, including (1) applying stiff structures of the spiro-locked acceptor and the sterically restricted donor that minimize structural relaxation, (2) introducing intermolecular HBs that optimize the D–A interactions and (3) fine-tuned D : A weight ratios which constrain concentration quenching. Apart from the higher EQE$_{max}$s, it is noteworthy that devices A1 and B had small efficiency roll-offs of 18.9%/39.1%/49.2% and 21.3%/38.3%/47.5%, respectively, at 100/500/1000 cd m^{-2}. In sharp contrast, EQEs of devices C–F decreased much faster that drop rates of EQE$_{100}$ vary from 57.6% to 69.6%, which can be ascribed to the triplet–triplet annihilation and triplet–polaron annihilation induced by the longer τ_{d} of **TPA-2NP**- and **TPA-QP**-based exciplexes.

To demonstrate the positive effect of TADF-characterized components on the exciton utilization, 11-([1,1′:3′,1″-ter-phenyl]-5′-yl)dipyrido[3,2-a:2′,3′-c]phenazine (TPh-2NP) was designed and synthesized for comparison purposes (Fig. S24†) by replacing TPA with terphenyl. Only a nanosecond-scale lifetime was observed, suggesting its locally excited characteristics. Demonstrating a similar rigidity to that of **TPA-2NP** (Fig. S24a;† the relatively small RMSD$_{S1–T1}$ may be due to both S$_1$ and T$_1$ being locally excited states), the EQE$_{max}$ of the **mPTBC : TPh-2NP**-based device is 5.2%, less than half of that of **mPTBC : TPA-2NP** (Fig. S25†), indicating that the introduction of TADF components greatly improves the exciton utilization.[50] Compared with blue and green emissions, such a positive effect may be amplified in the long-wavelength region where the non-radiative decay becomes overwhelming.[8,16]

Finally, the operational stability of the six exciplex emitters was studied using a device structure of ITO/NPB (40 nm)/Tris-PCz (10 nm)/EML (20 nm)/SF3-TRZ(10 nm)/SF3-TRZ : Liq (7 : 3, 50 nm)/Liq (2 nm)/Al (100 nm). The EML is consistent with those of devices A1 and B–F. As shown in Fig. S26,† LT$_{50}$ (time corresponding to 50% of the initial luminance) values at 500 cd m^{-2} of **mPTBC : SAF-2NP**, **mPTZC : SAF-2NP**, **mPTBC : TPA-2NP**, **mPTBC : TPA-QP**, **mPTZC : TPA-2NP** and **mPTZC : TPA-QP** are 349, 213, 186, 157, 153 and 92 hours, following the same trend as their EQE$_{max}$s in Table 2. The longer lifetimes of **SAF-2NP**-based exciplex emitters may originate from their shorter exciton lifetimes[51] as mentioned in the photophysical study.

Conclusions

In conclusion, we have elucidated that the rigidity of molecular structures, the interactions between D and A molecules as well as D–D/A–A interactions are influential in the non-radiative decay of exciplex emitters. By constructing a rigid system featuring stiff structures that inhibit structural relaxation, HBs which optimize intermolecular interactions and a fine-tuned D : A mixing ratio, the proof-of-concept exciplex emitter **mPTBC : SAF-2NP** showed a 3.3-fold higher Φ_{PL} (84.1%) and a 70% lower k_{nr} (1.98 × 10^{6} s^{-1}) than the comparison group. **mPTBC : SAF-2NP** also achieved outstanding EL performance, showing a superior EQE$_{max}$ of 23.8% with an emission peak of

608 nm, which represents a significant advancement over previously reported red OLEDs based on exciplex emitters. The present work provides a comprehensive understanding of non-radiative decay paths of exciplex emitters and can be a guide for developing efficient multicomponent emitting systems.

Data availability

All experimental and calculational data are available from the corresponding author upon reasonable request.

Author contributions

H.-Y. Z. led the investigation, conducted formal analysis and wrote the original draft. M. Z. and H. Z. helped with the data curation and validation. H.-Y. Y. helped with the investigation (synthesis). B. H. contributed to formal analysis and funding acquisition. Y.-H. Z. contributed to formal analysis and methodology. H. W. helped with the methodology. S.-L. T. and H. L. helped review and edit the manuscript. C.-J. Z. conceptualized, supervised and funded the project. X.-H. Z. helped review the manuscript and provided funding.

Conflicts of interest

There are no conflicts to declare.

Acknowledgements

Notes and references

1 B. Hu, Z. Yang and F. E. Karasz, *J. Appl. Phys.*, 1994, **76**, 2419–2422.

2 K. Goushi, K. Yoshida, K. Sato and C. Adachi, *Nat. Photonics*, 2012, **6**, 253–258.

3 M. Zhang, C.-J. Zheng, H. Lin and S.-L. Tao, *Mater. Horiz.*, 2021, **8**, 401–425.

4 M. Sarma, L.-M. Chen, Y.-S. Chen and K.-T. Wong, *Mater. Sci. Eng., R*, 2022, **150**, 100689.

5 X.-K. Liu, Z. Chen, C.-J. Zheng, C.-L. Liu, C.-S. Lee, F. Li, X.-M. Ou and X.-H. Zhang, *Adv. Mater.*, 2015, **27**, 2378–2383.

6 M. Wang, Y. Huang, K. Lin, T. Yeh, J. Duan, T. Ko, S. Liu, K. Wong and B. Hu, *Adv. Mater.*, 2019, **31**, 1904114.

7 T.-C. Lin, M. Sarma, Y.-T. Chen, S.-H. Liu, K.-T. Lin, P.-Y. Chiang, W.-T. Chuang, Y.-C. Liu, H.-F. Hsu, W.-Y. Hung, W.-C. Tang, K.-T. Wong and P.-T. Chou, *Nat. Commun.*, 2018, **9**, 3111.

8 M. Zhang, W. Liu, C. Zheng, K. Wang, Y. Shi, X. Li, H. Lin, S. Tao and X. Zhang, *Adv. Sci.*, 2019, **6**, 1801938.

9 J. Zhao, C. Zheng, Y. Zhou, C. Li, J. Ye, X. Du, W. Li, Z. He, M. Zhang, H. Lin, S. Tao and X. Zhang, *Mater. Horiz.*, 2019, **6**, 1425–1432.

10 Z. Zhang, D. Dou, R. Xia, P. Wu, E. Spuling, K. Wang, J. Cao, B. Wei, X. Li, J. Zhang, S. Bräse and Z. Wang, *Sci. Adv.*, 2023, **9**, eadf4060.

11 N. R. Al Amin, K. K. Kesavan, S. Biring, C.-C. Lee, T.-H. Yeh, T.-Y. Ko, S.-W. Liu and K.-T. Wong, *ACS Appl. Electron. Mater.*, 2020, **2**, 1011–1019.

12 T.-L. Wu, S.-Y. Liao, P.-Y. Huang, Z.-S. Hong, M.-P. Huang, C.-C. Lin, M.-J. Cheng and C.-H. Cheng, *ACS Appl. Mater. Interfaces*, 2019, **11**, 19294–19300.

13 Y. Qin, P. Tao, L. Gao, P. She, S. Liu, X. Li, F. Li, H. Wang, Q. Zhao, Y. Miao and W. Huang, *Adv. Opt. Mater.*, 2019, **7**, 1801160.

14 W.-Y. Hung, G.-C. Fang, S.-W. Lin, S.-H. Cheng, K.-T. Wong, T.-Y. Kuo and P.-T. Chou, *Sci. Rep.*, 2014, **4**, 5161.

15 M. Zhang, C.-J. Zheng, H.-Y. Zhang, H.-Y. Yang, K. Wang, Y.-Z. Shi, H. Lin, S.-L. Tao and X.-H. Zhang, *J. Mater. Chem. C*, 2022, **10**, 15593–15600.

16 Y. Hu, Y. Yu, Y. Yuan, Z. Jiang and L. Liao, *Adv. Opt. Mater.*, 2020, **8**, 1901917.

17 R. Englman and J. Jortner, *Mol. Phys.*, 1970, **18**, 145–164.

18 J. H. Kim, J. H. Yun and J. Y. Lee, *Adv. Opt. Mater.*, 2018, **6**, 1800255.

19 Q. Zhang, H. Kuwabara, W. J. Potscavage, S. Huang, Y. Hatae, T. Shibata and C. Adachi, *J. Am. Chem. Soc.*, 2014, **136**, 18070–18081.

20 H.-Y. Yang, H. Zhang, M. Zhang, X. Fan, H. Lin, S.-L. Tao, C.-J. Zheng and X.-H. Zhang, *Chem. Eng. J.*, 2022, **448**, 137717.

21 C.-Y. Lin, C.-H. Hsu, C.-M. Hung, C.-C. Wu, Y.-H. Liu, E. H.-C. Shi, T.-H. Lin, Y.-C. Hu, W.-Y. Hung, K.-T. Wong and P.-T. Chou, *Nat. Chem.*, 2024, **16**, 98–106.

22 A. Chand, D. K. Sahoo, A. Rana, S. Jena and H. S. Biswal, *Acc. Chem. Res.*, 2020, **53**, 1580–1592.

23 S. Emamian, T. Lu, H. Kruse and H. Emamian, *J. Comput. Chem.*, 2019, **40**, 2868–2881.

24 R. Lin, J. Liu, W. Xu, Z. Liu, X. He, C. Zheng, M. Kang, X. Li, Z. Zhang, H.-T. Feng, J. W. Y. Lam, D. Wang, M. Chen and B. Z. Tang, *Adv. Mater.*, 2023, **35**, 2303212.

25 D.-Q. Wang, M. Zhang, K. Wang, C.-J. Zheng, Y.-Z. Shi, J.-X. Chen, H. Lin, S.-L. Tao and X.-H. Zhang, *Dyes Pigm.*, 2017, **143**, 62–70.

26 H.-Y. Zhang, H.-Y. Yang, M. Zhang, H. Lin, S.-L. Tao, C.-J. Zheng and X.-H. Zhang, *Mater. Horiz.*, 2022, **9**, 2425–2432.

27 C. B. Larsen, H. van der Salm, C. A. Clark, A. B. S. Elliott, M. G. Fraser, R. Horvath, N. T. Lucas, X.-Z. Sun, M. W. George and K. C. Gordon, *Inorg. Chem.*, 2014, **53**, 1339–1354.

28 C. Si, A. K. Gupta, B. Basumatary, A. P. McKay, D. B. Cordes, A. M. Z. Slawin, I. D. W. Samuel and E. Zysman-Colman, *Adv. Funct. Mater.*, 2024, **34**, 2315935.

29 J. Xue, Q. Liang, R. Wang, J. Hou, W. Li, Q. Peng, Z. Shuai and J. Qiao, *Adv. Mater.*, 2019, **31**, 1808242.

30 C. Li, R. Duan, B. Liang, G. Han, S. Wang, K. Ye, Y. Liu, Y. Yi and Y. Wang, *Angew. Chem., Int. Ed.*, 2017, **56**, 11525–11529.

31 M. Cocchi, D. Virgili, G. Giro, V. Fattori, P. Di Marco, J. Kalinowski and Y. Shirota, *Appl. Phys. Lett.*, 2002, **80**, 2401–2403.

32 M. J. Frisch, G. W. Trucks, H. B. Schlegel, G. E. Scuseria, M. A. Robb, J. R. Cheeseman, G. Scalmani, V. Barone, G. A. Petersson, H. Nakatsuji, X. Li, M. Caricato, A. V. Marenich, J. Bloino, B. G. Janesko, R. Gomperts, B. Mennucci, H. P. Hratchian, J. V. Ortiz, A. F. Izmaylov, J. L. Sonnenberg, D. Williams-Young, F. Ding, F. Lipparini, F. Egidi, J. Goings, B. Peng, A. Petrone, T. Henderson, D. Ranasinghe, V. G. Zakrzewski, J. Gao, N. Rega, G. Zheng, W. Liang, M. Hada, M. Ehara, K. Toyota, R. Fukuda, J. Hasegawa, M. Ishida, T. Nakajima, Y. Honda, O. Kitao, H. Nakai, T. Vreven, K. Throssell, J. A. Montgomery Jr, J. E. Peralta, F. Ogliaro, M. J. Bearpark, J. J. Heyd, E. N. Brothers, K. N. Kudin, V. N. Staroverov, T. A. Keith, R. Kobayashi, J. Normand, K. Raghavachari, A. P. Rendell, J. C. Burant, S. S. Iyengar, J. Tomasi, M. Cossi, J. M. Millam, M. Klene, C. Adamo, R. Cammi, J. W. Ochterski, R. L. Martin, K. Morokuma, O. Farkas, J. B. Foresman and D. J. Fox, *Gaussian 16 Rev. A.03.*, Wallingford, CT, 2016.

33 W. Humphrey, A. Dalke and K. Schulten, *J. Mol. Graphics*, 1996, **14**, 33–38.

34 J. R. Reimers, *J. Chem. Phys.*, 2001, **115**, 9103–9109.

35 M. Zhang, C. Zheng, K. Wang, Y. Shi, D. Wang, X. Li, H. Lin, S. Tao and X. Zhang, *Adv. Funct. Mater.*, 2021, **31**, 2010100.

36 X. Du, X. Lu, J. Zhao, Y. Zhang, X. Li, H. Lin, C. Zheng and S. Tao, *Adv. Funct. Mater.*, 2019, **29**, 1902078.

37 T. Lu and Q. Chen, *J. Comput. Chem.*, 2022, **43**, 539–555.

38 T. Lu and F. Chen, *J. Comput. Chem.*, 2012, **33**, 580–592.

39 J. Zhang and T. Lu, *Phys. Chem. Chem. Phys.*, 2021, **23**, 20323–20328.

40 V. Jankus, P. Data, D. Graves, C. McGuinness, J. Santos, M. R. Bryce, F. B. Dias and A. P. Monkman, *Adv. Funct. Mater.*, 2014, **24**, 6178–6186.

41 W.-Y. Hung, G.-C. Fang, Y.-C. Chang, T.-Y. Kuo, P.-T. Chou, S.-W. Lin and K.-T. Wong, *ACS Appl. Mater. Interfaces*, 2013, **5**, 6826–6831.

42 B. Zhao, T. Zhang, B. Chu, W. Li, Z. Su, Y. Luo, R. Li, X. Yan, F. Jin, Y. Gao and H. Wu, *Org. Electron.*, 2015, **17**, 15–21.

43 D. Chen, G. Xie, X. Cai, M. Liu, Y. Cao and S. Su, *Adv. Mater.*, 2016, **28**, 239–244.

44 G. Grybauskaite-Kaminskiene, K. Ivaniuk, G. Bagdziunas, P. Turyk, P. Stakhira, G. Baryshnikov, D. Volyniuk, V. Cherpak, B. Minaev, Z. Hotra, H. Ågren and J. V. Grazulevicius, *J. Mater. Chem. C*, 2018, **6**, 1543–1550.

45 G. Liu, T. Huang, H. Wang, C. Hsu, P. Chou, W. Hung and K. Wong, *Chem.–Eur. J.*, 2023, **29**, e202203660.

46 M. Chapran, P. Pander, M. Vasylieva, G. Wiosna-Salyga, J. Ulanski, F. B. Dias and P. Data, *ACS Appl. Mater. Interfaces*, 2019, **11**, 13460–13471.

47 Y. Zhang, Q. Ran, Q. Wang, Y. Liu, C. Hänisch, S. Reineke, J. Fan and L. Liao, *Adv. Mater.*, 2019, **31**, 1902368.

48 Z. Cai, X. Wu, H. Liu, J. Guo, D. Yang, D. Ma, Z. Zhao and B. Z. Tang, *Angew. Chem., Int. Ed.*, 2021, **60**, 23635–23640.

49 H. Wang, K. Wang, J. Chen, X. Zhang, L. Zhou, X. Fan, Y. Cheng, X. Hao, J. Yu and X. Zhang, *Adv. Funct. Mater.*, 2023, **33**, 2304398.

50 W. Liu, J.-X. Chen, C.-J. Zheng, K. Wang, D.-Y. Chen, F. Li, Y.-P. Dong, C.-S. Lee, X.-M. Ou and X.-H. Zhang, *Adv. Funct. Mater.*, 2016, **26**, 2002–2008.

51 L.-S. Cui, A. J. Gillett, S.-F. Zhang, H. Ye, Y. Liu, X.-K. Chen, Z.-S. Lin, E. W. Evans, W. K. Myers, T. K. Ronson, H. Nakanotani, S. Reineke, J.-L. Bredas, C. Adachi and R. H. Friend, *Nat. Photonics*, 2020, **14**, 636–642.